Journal of Statistical Physics, Vol. 52, Nos. 5/6, 1988

Monte Carlo Analysis of the Internal Structure of Light Scattering Particles with Slit-Scan Illumination

R. Bhandari[1,2] **and M. Kerker**[1]

Received March 30, 1988

An algorithm based upon a Monte Carlo procedure for calculating the scattering and absorption by a host particle containing a distribution of particulate inclusions is described. The host particle is sufficiently large so that ray optics can be applied. The inclusions are too small for ray optics but sufficiently large so that the full boundary-value formalism must be used. A major consideration is to determine whether the internal structure is better resolved when slit-scan illumination is utilized rather than plane wave illumination. The algorithm is tested for a layered sphere for which the boundary value solution is available.

KEY WORDS: Light scattering; slit-scan illumination; flow cytometry; particle size; particle structure; Monte Carlo light scattering analysis; biological cell structure; light absorption by particles.

Howard Reiss' wide-ranging contributions to physical chemistry and to colloid science go back more than 40 years when he and one of us (M. K.) were fellow graduate students. It is a joy to dedicate this paper to him on the occasion of his 66th birthday.

1. INTRODUCTION

Lord Rayleigh's great body of analysis[1),3] has provided the point of departure for understanding light scattering phenomena. As his work has been

[1] Clarkson University, Potsdam, New York 13676.

[2] Present address: AT&T Bell Laboratories, Holmdel, New Jersey 07733.

[3] Lord Rayleigh's contribution covered dipolar scattering, the boundary value solution (for cylinders), the integral equation solution (including the presently so-called first- as well as higher-order Born approximation), the optical theorem solution (which Debye applied to polymer molecular weight determination), and Doppler-shifted dipolar emission (which underlies quasistatic scattering).

0022-4715/88/0900-1263$06.00/0

further developed[4] and as modern computational techniques have been implemented, the hope has been that light scattering might provide a powerful diagnostic technique that would permit the determination of particle size, shape, and internal structure. Unfortunately, that hope has been only partly realized. The problem is that the experimental data are normally too ill conditioned for numerical inversion even when the particle scattering theory is available. This state of affairs is aggravated whenever dispersions are treated having a distribution of size, shape, and orientation. The information content is degraded because the signals represent averages over these distributions. This particular difficulty may be overcome to some extent by experimental techniques which permit rapid processing of signals from individual particles flowing in single file through a light beam.[3,4] Indeed, interrogation of fluorescent light scattering signals from single stained biological cells in flow is extensively used heuristically to identify abnormal cells in a population of normal cells.[5,6]

Biological cells, as well as many inert particles, possess an internal structure which alters the elastic light scattering signals so that deconvolution of these suggests a possibility for describing such structures, or at least of identifying or discriminating among categories of particles. A simple configuration such as a layered sphere is amenable to theoretical analysis[7] and for this reason a biological cell has been modeled as a spherical nucleus centered within a cytoplasmic sphere,[8,9] an absorbing atmospheric cloud droplet as a graphite core embedded within a water drop[10] or as a multilayered sphere consisting of a water core, carbon shell, and a water shell,[11] an exploding spray droplet from a coal-water slurry as a multilayered sphere consisting of a coal core, a layer of water and an outer layer of expanding water vapor,[12] etc. But inversion of the data from such heterogeneous particles is even more subject to the kinds of instabilities that plague homogeneous droplets.

Moreover, for structures more complex and more realistic than concentric layered spheres, there remains the primary question of how to calculate their scattering and absorption.

We attempted to extend the layered sphere model to a sphere with a somewhat less regular internal structure.[13] The internal field was approximated by that of a homogeneous sphere whose dielectric constant was obtained from the volume-weighted polarizability of the actual structure. This field was then used to pump the actual distribution of polarizable dipoles and the scattered field was obtained with the aid of Saxon's integral formulation of the scattered field.[14] This approximation, in the test case of

[4] Ref. 2 is a compilation of 97 papers which have extended and amplified the classical papers published during the first decades of this century.

a layered sphere, agreed with the boundary value solution only for small differences in the polarizability and for relatively small particles. Thus, it did not prove useful either for biological cells or for the cloud and spray droplets to which we have just referred.

There have been other attempts, in which a structured particle is modeled by a similar homogeneous particle for which the dielectric constant is obtained by an effective-medium approach.[15] Bohren[16] has discussed the aplicability of effective-medium theories to scattering and absorption by inhomogeneous particles and has shown in a general way that even when the inclusions are of moderate size such theories lead necessarily to erroneous results. We might consider more specifically how obvious this error becomes whenever the inclusions are absorptive. The distribution of heat sources within a homogeneous particle is highly irregular, depending upon particle size and refractive index. With absorbing inclusions distributed within a nonabsorbing host, the heat sources are necessarily localized within the inclusions, whereas homogenizing the particle by an effective-medium theory distributes these sources throughout the particle quite independently of the location of the inclusions. This would lead to obviously erroneous results for phenomena dependent upon the location of the absorption centers such as photophoresis or photoelectron emission. There would be no connection between the absorption or scattered signals and the actual internal structure of the particle.

In this paper we propose and test a new algorithm applicable to a structured particle large enough for geometrical optics to be appropriate at the surface but with smaller particulate inclusions whose sizes comparable to the wavelength necessitate the full boundary value treatment. Many biological cells as well as many cloud droplets containing graphitic particulates correspond to this model. The incident beam is resolved into a sequence of rays each of whose life history upon impinging on the particle is treated by a Monte Carlo procedure. However, before describing the algorithm it will be usefull to consider the technique of slit-scan illumination. This experimental technique offers the possibility of enhancing the resolution of internal structure and it may be combined in a very natural way with the Monte Carlo algorithm.

2. SLIT-SCAN LIGHT SCATTERING

In the preponderance of light scattering studies, the particle is totally immersed in the illuminating beam, an unavoidable consequence when dealing with micrometer and submicrometer particles. This may be termed "zero-resolution" illumination in contrast to optical or transmission electron microscopy, also based upon scattering, which permits resolution to

the magnitude of the wavelength. Theoretical light scattering studies are based upon illumination by either a plane wave or a shaped beam which completely envelops the particle, i.e., zero-resolution illumination. Light scattering signals for zero-resolution illumination are coherently averaged over the internal structure. This leads to the well-known instabilities encountered whenever attempting to invert averaged signals to, uncover the primary structure.

When the illuminating beam is focused down to a narrow slit with a dimension much smaller than the particle, morphological information is better resolved, at least to the dimension of the slit. Such intermediate-resolution illumination is termed slit-scanning, particularly if the information is processed sequentially as the particle traverses the beam. Such a traverse provides a slit-scan contour. The technique has been applied to biological cells whose nuclei and cytoplasm are separately stained with fluorescent dyes. Wheeless, who has pioneered the technique,[17] has recently developed multidimensional instrumentation utilizing three laser beams focused to micrometer Gaussian waists which intersect the particle orthogonally, thereby providing a tomographic view.[18] A schematic diagram of the flow and the fluorescent signal is given in Fig. 1. It is apparent the slit-scan fluorimetry provides highly resolved information in this case on cell and nuclear boundaries. Wheeless has recently undertaken to extend this technique to elastic light scattering signals, and the elucidation of such signals has provided some of the motivation for the present study.

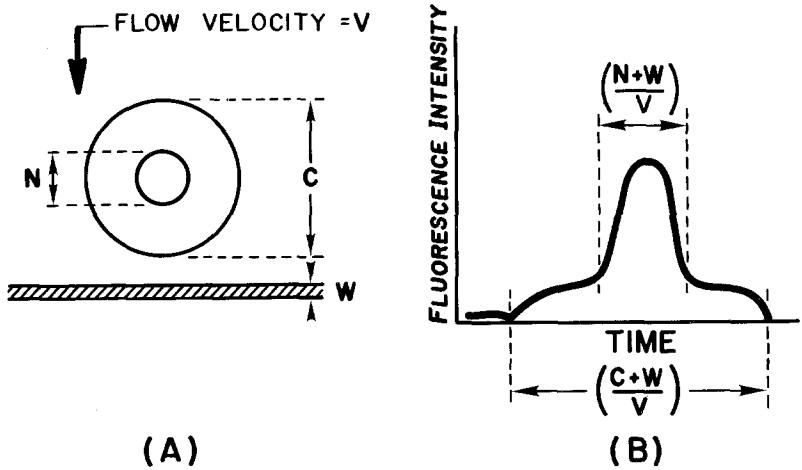

Fig. 1. (A) Biological cell flowing through slit-scan illumination and (B) resulting slit-scan fluorescence contour. Cell and nuclear boundaries may be determined from the slit-scan fluorescence contour. N, Nuclear diameter; C, cell diameter; W, illumination slit width; V, flow velocity.

3. THE MODEL

The geometry shown in Fig. 2 is for illumination propagating along the positive z axis. A square detector with edge a at polar coordinates R, θ, ϕ subtends solid angle $\Delta\Omega = \sin\theta\,\Delta\theta\,\Delta\phi$, where $\Delta\phi = a/R\sin\theta$ and $\Delta\theta = a/R$. This detector geometry becomes important for the discussion of slit-scan illumination. In this paper, the detector will be taken to lie in the yz plane, i.e., $\phi = 90°$. The slit geometry is shown in Fig. 3. In this paper h will be taken parallel to the y axis.

The host particle is large enough so that in the absence of inclusions an accurate description of the scattering and absorption may be obtained by utilizing ray optics to account for reflections and refractions at the boundary together with transmissivity within the homogeneous particle as well as Fraunhofer diffraction around the outside. The inclusions, located at specific sites, are large enough to require application of the full boundary value treatment but not so large that the ray optics–diffraction approach can be used.

This initial investigation assumes that both the host and inclusions are concentric spheres and that the radiation scattered by the inclusion is unpolarized. Since the boundary value solution for this configuration is well known, it will permit testing of the ray optics and Monte Carlo approximations. The requisite formulas for the ray optics and the boundary value solution are given by van de Hulst[19] and elsewhere.[20]

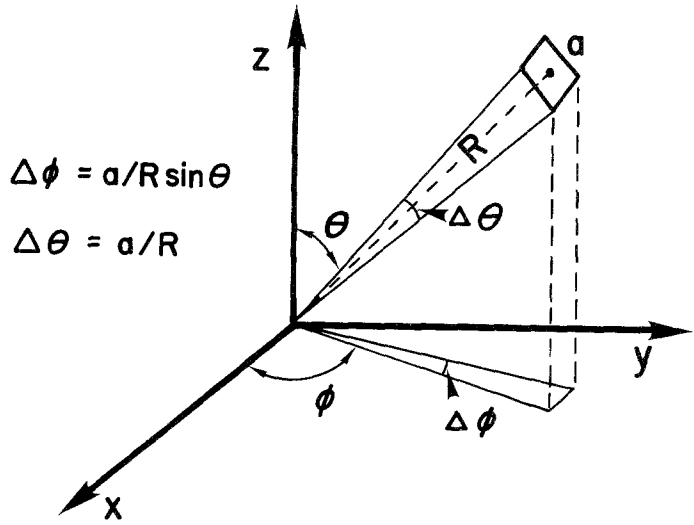

Fig. 2. Geometry. The beam propagates in the positive z direction. A square detector with side a subtends solid angle $\Omega = \sin\theta\,\Delta\theta\,\Delta\phi$, where $\Delta\phi = a/R\sin\theta$ and $\Delta\theta = a/R$.

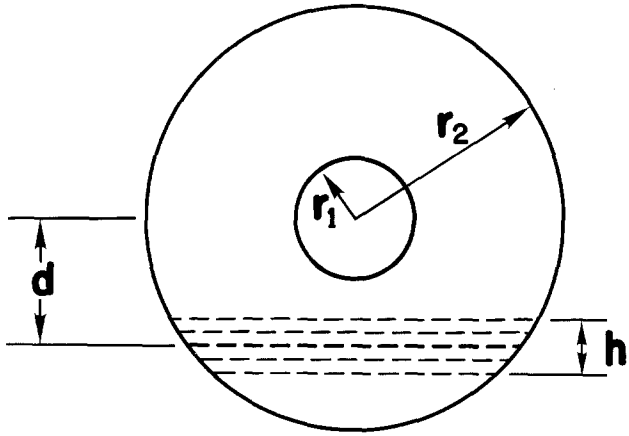

Fig. 3. Slit-scan illumination. The beam impinging on the layered sphere with radii r_1 and r_2 has height h and its center is distance d from the center.

The trajectory of a photon is followed by a Monte Carlo procedure from the source beam to termination at a detector located at observation points in the far field outside the host particle or at a particular inclusion, where the photon may be absorbed and either degraded to heat or reemitted at some shifted frequency (fluorescence or Raman scattering).

The scheme is outlined in Fig. 4 where an incident ray (S) along which the photon travels in the positive z direction is selected randomly. For plane wave illumination, which has been termed zero-resolution illumination, selection is made from the circular bundle of rays impinging on the particle. For slit-scan illumination selection is made from a bundle of rays of height h (Fig. 3) impinging on the particle whose central ray is at distance d from the center. A slit-scan contour is obtained by varying d from $(r_2 + h/2)$ to $-(r_2 + h/2)$.

Upon impact at the boundary B a decision is made probabilistically based upon Fresnel's equations on whether the photon is reflected (R_l) or refracted (R_r). In the former case the photon proceeds to an appropriate detector (D). Otherwise it follows the path of the refracted ray deterministically until it encounters an inclusion particle (P) or the boundary (B). In Fig. 4 a dashed line indicates a trajectory which was arrived at probabilistically; a solid line indicates a deterministic trajectory. A photon is deemed to encounter an inclusion if it passes within a circle concentric with the particle whose area is equal to the extinction cross section σ_{ext}. The extinction cross section is usually larger than the geometrical cross section.

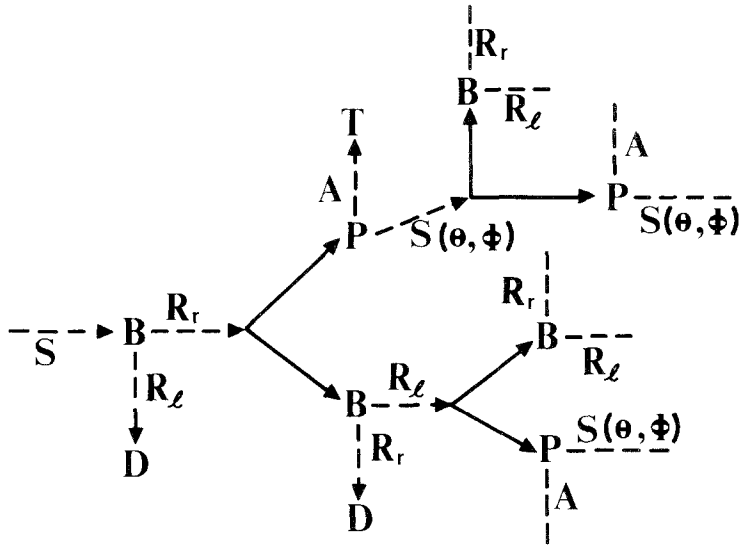

Fig. 4. Course of a photon through a heterogeneous particle. Dashed lines represent probabilistic decisions; solid lines represent deterministic decisions. *A*, Absorption; *B*, boundary; *D*, detector; *P*, particle; R_l, reflection; R_r, refraction; *S*, select incident ray; $S(\theta, \phi)$ scattering; *T*, termination by absorption.

If the first encounter within the host is with an inclusion particle, a probabilistic decision based upon the boundary value solution is made to determine whether the photon is absorbed (A) or scattered into a particular direction [$S(\theta, \phi)$]. Absorption terminates this photon (T). Scattering leads the photon along a deterministic path either to another inclusion particle or to the boundary, where the appropriate probabilistic events recur.

On the other hand, if the first encounter of the photon within the host particle is with the boundary, a probabilistic decision is made based upon Fresnel's equations. This leads the photon either to refract out of the host particle to a detector or upon reflection along a deterministic ray, to encounter either an inclusion particle or the boundary.

The process continues until the photon is absorbed or detected. If the host particle is lossy, the photon is attenuated accordingly along its trajectory. A sufficient number of tries N_0 is made until a stable result is obtained. Normally, for the parameters used here, $N_0 = 10^6$ was sufficient.

In the remainder of this paper, we will test the efficacy of this procedure for a homogeneous sphere and then for a sphere with a single spherical inclusion located at the center, using plane wave illumination.

Each of these results can be compared with exact boundary value solutions. Finally, the effect of slit-scan illumination will be explored in order to determine whether enhanced resolution is obtained.

4. MONTE CARLO SIMULATION OF SCATTERING OF LIGHT BY A HOMOGENEOUS SPHERE IN THE GEOMETRICAL OPTICS APPROXIMATION

The Monte Carlo approach to the scattering of light in the geometrical optics approximation was first tested by applying it to a homogeneous, nonabsorbing sphere. In geometrical optics, a beam of light is considered to be a collection of rays, each of which acts independently of the other.

Figure 5 shows a ray incident on a homogeneous (nonabsorbing) sphere with radius a and its emergence after impact as a series of rays labeled $p = 0, 1, 2, \ldots$. At each interface A, B, C,..., the ray separates into a reflected and refracted ray. The division of energy is determined by Fresnel coefficients.

In the Monte Carlo scheme, the ray's total (initial) energy is preserved. Accordingly, at each interface, it is presumed to be either totally reflected or totally refracted, the probability of each event determined by the Fresnel coefficients. More specifically, the Monte Carlo treatment consists of the following.

1. A random number ξ in the range 0 to 1 is selected. The impact parameter b of a ray is then determined by the expression

$$b = \xi^{1/2} a \tag{1}$$

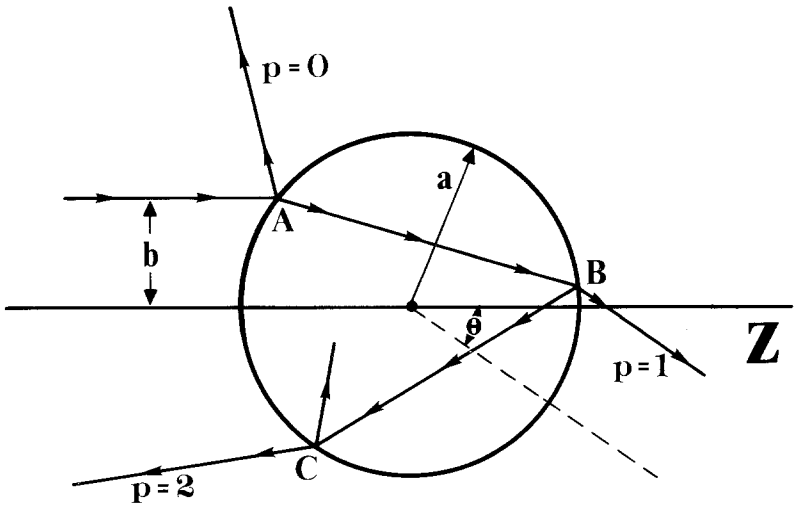

Fig. 5. Ray tracing for scattering by a homogeneous sphere.

where a is the radius of the sphere. Consideration of azimuthal angle ϕ of the ray is redundant because of azimuthal symmetry of the problem at this time.

2. At point of impact A, the ray is either reflected or refracted. What happens precisely is determined in the following manner: A random number ξ is again selected. If (a) $0 < \xi < r^2$, the ray is reflected; if (b) $r^2 < \xi < 1$, the ray is refracted into the sphere. The parameter r is the Fresnel reflection coefficient. Its value is

$$r_1 = \frac{\sin \tau - m \sin \tau'}{\sin \tau + m \sin \tau'} \tag{2a}$$

for polarization of type 1 (polarization of incident ray perpendicular to the scattering plane) and

$$r_2 = \frac{m \sin \tau - \sin \tau'}{m \sin \tau + \sin \tau'} \tag{2b}$$

for polarization of type 2 (polarization of incident ray parallel to the scattering plane), where

$$\tau = \cos^{-1}(b/a)$$
$$\tau' = \cos^{-1}(b/ma) \tag{3b}$$

and m is the refractive index of the sphere.

In what follows, we assume that the polarization is always of type 1. Rays of type 2 can be dealt with in a similar fashion.

3. If case (a) occurs, information is recorded and the whole process is repeated with a new ray generated in step 1.

If case (b) is true, the ray travels inside the sphere in a direction in accordance with Snell's law. At its next impact point B, whether it is reflected into or refracted out as a $p = 1$ ray is again decided by the selection of a new random number. The probability of reflection for the ray within the particle is the same as the probability of reflection when the ray strikes from the outside.

4. If in the above game of chance the ray remains trapped inside the sphere, the process is terminated after it has undergone four internal reflections. Such a ray is considered lost. No significant error results, as such events are very rare.

5. The scattering angle θ for an emerging ray characterized by a certain value p is calculated from the relation

$$2\tau - 2p\tau' = 2\pi l + q\theta \tag{4}$$

where l is an integer. q is assigned the value of $+1$ or -1 to ensure that θ lies between 0 and π. Figure 5 depicts the scattering angle θ for the $p = 1$ ray.

Steps 1–5 are repeated N_0 times, where N_0 is a large number. Thus, the path history of N_0 different rays is recorded. The entire procedure above can be repeated for the other type of polarization, using Fresnel reflection coefficient r_2.

Calculations were performed for a water droplet (refractive index $m = 1.33$). Table I shows the fraction of incident energy scattered by a water droplet for polarization 1 in which the electric vector vibrates perpendicular to the scattering plane. Values obtained by van de Hulst[18] by a direct computation of the geometrical optics expressions are also indicated. The agreement between the two sets of values is in general excellent with errors of the order of 1 % or less, except in the cases of very low fractions (which is expected). Similar results were obtained for polarization 2.

If $N(\theta)$ denotes the number of optical particles (rays) scattered in a small interval $\Delta\theta$ around θ, then in terms of the differential cross section $d\sigma_{sca}/d\theta$, where σ_{sca} is the scattering cross section,

$$\frac{N(\theta)}{N_0} \equiv \frac{1}{\pi a^2} \frac{d\sigma_{sca}}{d\theta} \Delta\theta \tag{5}$$

Figure 6 shows a plot of $N(\theta)/N_0$ versus θ (curve A) obtained from the Monte Carlo procedure with $N_0 = 1{,}000{,}000$. The interval $\Delta\theta = 1°$. Curve B, which is obtained from the right-hand side of Eq. (5), is calculated from boundary value theory for $a = 50\ \mu$m and $\lambda_0 = 0.5\ \mu$m (size parameter 628). Except for oscillations in curve B due to interference

Table I. Fraction of the incident Energy Scattered by a Water Droplet in Given Intervals of θ by Different Rays[a]

Interval of θ (deg)	0–30	30–60	60–90	90–120	120–150	150–180
Fraction$^{(M)}$	0.5836	0.2962	0.0315	0.0112	0.0650	0.0104
Fraction$^{(H)}$	0.5790	0.3002	0.0326	0.0114	0.0660	0.0108
Value of p						
Fraction$^{(M)}$	0.1010	0.8233	0.0613	0.0096	0.0027	0.0023
Fraction$^{(H)}$	0.1020	0.8217	0.0617	0.0098	0.0026	0.0022

[a] Superscripts (M) and (H) indicate values obtained by the Monte Carlo procedure and by van de Hulst, respectively. $N_0 = 1{,}000{,}000$.

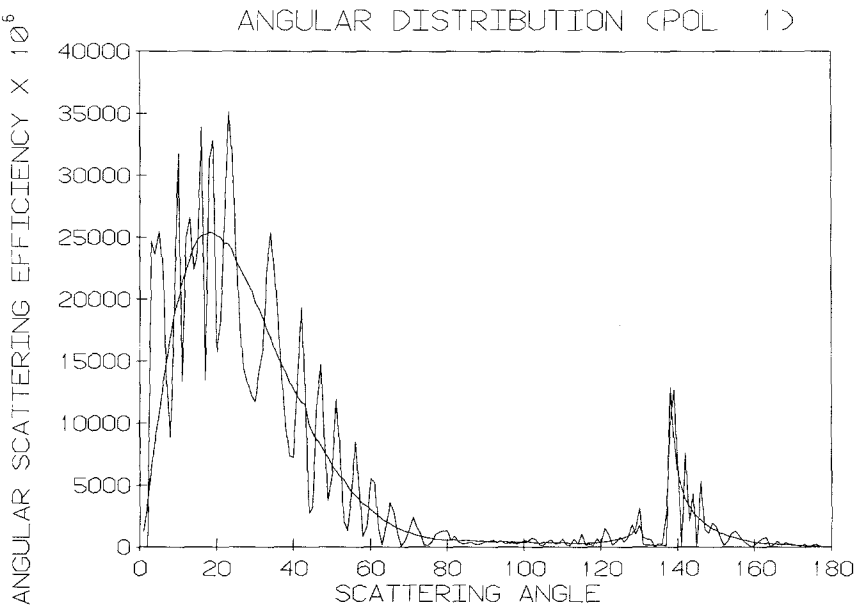

Fig. 6. Comparison of Monte Carlo simulation of scattering with the boundary value solution for a 50-μm-radius sphere, $m = 1.33$, $\lambda_0 = 0.5$ μm.

effects,[5] there is good agreement between the Monte Carlo results based ion geometrical optics and the general trend for the boundary value theory. The Monte Carlo procedure does not exhibit the oscillatory structure because it does not take interference into account. This defect can be remedied by tracking phase and including interference. However, the general envelope obtained by neglecting phase will suffice for most experimental applications. Also, it should be noted that the forward lobe which is usually so apparent in angular scattering plots is suppressed in this case because we have chosen to present $d\sigma_{sca}/d\theta$ rather than $d\sigma_{sca}/d(\cos\theta)$.

The peaks at $\theta \approx 129°$ and $\theta \approx 138°$ are the rainbows predicted by geometrical optics. Mathematically, they correspond to $d\theta/d\tau = 0$. The one at $\theta \approx 129°$ is due to the $p = 3$ rays and the one at $\theta \approx 138°$ corresponds to the $p = 2$ rays. The weak rainbow corresponding to $p = 4$ which is predicted

[5] The forward diffraction peak is confined to an angle $< 0.4°$ and is not shown. The actual oscillations predicted by Mie theory are much narrower. The separation between two consecutive maxima is about $180°/x \approx 0.3°$. Thus, the detailed structure can only be revealed by making the step size smaller than 0.3°. We have verified this.

to occur at $\theta \approx 41^\circ$ is visible only as a smaller shoulder. Indeed, when N_0 was increased to 2,000,000, it showed up more prominently, confirming its existence. Somewhat similar results were obtained for polarization 2.

5. ABSORPTION BY A LAYERED SPHERE CONTAINING AN ABSORBING CORE

In this section we investigate the absorption by a dielectric sphere containing an absorbing core by three methods: (1) boundary value theory, (2) a deterministic treatment in which geometrical optics is used to describe reflection–refraction at the sphere boundary whereas boundary value theory is used to describe absorption by the core, and (3) a Monte Carlo treatment of part 2.

Method 2 can be understood with reference to Fig. 7, where

$$b = a_2 \sin i, \qquad d = a_2 \sin i'$$

so that

$$b/d = \sin i / \sin i' = m_2$$

where a_2 and m_2 are the radius and refractive index of the shell, respectively. Thus, this focusing effect of the shell increases the intensity incident on the core by a factor m_2^2.

If σ'_{abs}, σ'_{sca}, and σ'_{ext} are, respectively, the absorption, scattering, and extinction cross sections of the core calculated from boundary value theory as if the core were embedded in an infinite medium of refractive index m_2, the absorption for unit irradiance is

$$m_2^2(1-r^2)\,\sigma'_{abs}$$

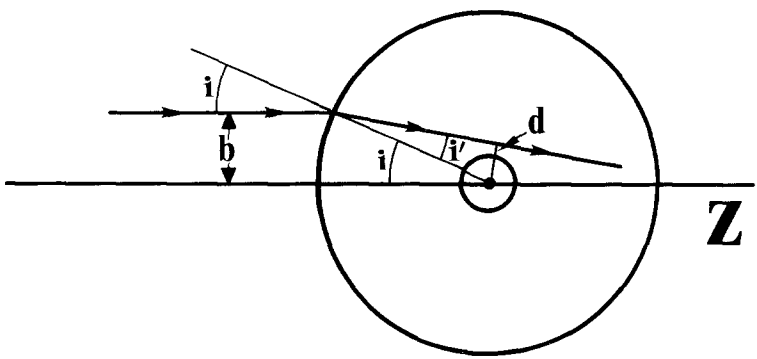

Fig. 7. Ray tracing for absorption by an inclusion in a layered sphere.

and the scattered radiance is

$$m_2^2(1\text{-}r^2)\,\sigma'_{\text{sca}}$$

where r denotes the Fresnel reflection coefficient.

Since $a_1 \ll a_2$, the light incident on the particle which interacts with the core has $i \approx 0°$. Consequently, $r \approx (1-m_2)/(1+m_2)$. A fraction r^2 of the light scattered by the core is reflected back on the core by the shell. This light is rescattered and rereflected back by the shell on the core, rescattered, and so on. Treating the scattering of a ray in a manner similar to the plane wave, the absorption of light for unit incident irradiance is

$$m_2^2(1-r^2)\,\sigma'_{\text{abs}}\left[1 + r^2\frac{\sigma'_{\text{sca}}}{\sigma'_{\text{ext}}} + r^4\left(\frac{\sigma'_{\text{sca}}}{\sigma'_{\text{ext}}}\right)^2 + \cdots\right] = \frac{m_2^2(1-r^2)\,\sigma'_{\text{abs}}}{1 - r^2\sigma'_{\text{sca}}/\sigma'_{\text{ext}}} \qquad (6)$$

For m_2 close to 1, $r^2 = (1-m_2)^2/(1+m_2)^2 \approx 0$. If the denominator is neglected, which is equivalent to ignoring absorption due to reflections from the shell, the fractional error is $r^2\sigma'_{\text{sca}}/\sigma'_{\text{ext}} < r^2$. For water ($m = 1.33$), $r^2 = 0.02$.

Tables II–IV compare results obtained under the above approximation with those obtained from the exact boundary value expressions for a layered sphere.[7,20] Tables III and IV include the Monte Carlo calculation for this approximation. These tables thereby provide a test of both the geometrical optics approximation and the Monte Carlo routine for computing it. From Table II, which explores the effect of the host particle size, deviations from the exact results become significant (>1 %) when

Table II. Effect of Host Particle Size (a_2) upon Absorption Cross Section per Unit Volume of the Core (m^2/cm^3) for a Single-Layered Sphere[a]

$a_2(\mu m)$	SL	A
50	1.401	1.403
5	1.396	1.403
2	1.386	1.403
1.5	1.396	1.403
1.35	1.331	1.403

[a] $m_1 = 2.0 - i0.66$ (graphitic carbon), $m_2 = 1.33$ (water), $a_1 = 1\ \mu m$, $\lambda_0 = 0.5\ \mu m$. SL and A refer to the results from the boundary value solution and the approximation method [Eq. (6)], respectively.

Table III. Effect of Host Particle Refractive Index (m_2) upon Absorption Cross Section per Unit Volume of the Core (m^2/cm^3) for a Single-Layered Sphere[a]

m_2	SL	A	M
1.13	1.013	1.017	1.019
1.33	1.386	1.403	1.399
1.53	1.796	1.821	1.788
1.83	2.392	2.471	2.367
2.03	2.784	2.889	2.717

[a] $m_1 = 2.0 - i0.66$, $a_1 = 1$ μm, $a_2 = 5$ μm, $\lambda_0 = 0.5$ μm. SL, A, and M refer to the results from the boundary value solution, the approximation method [Eq. (6)], and the Monte Carlo procedure ($N_0 = 1{,}000{,}000$), respectively.

$a_2 < 1.5$ μm. Thus, geometrical optics seems to work well even for values of a_2 this low. Table III explores the effect of host refractive index. It indicates that errors are negligible up to $m_2 = 1.23$, are about 1 % in the range $1.23 < m_2 < 1.53$, and become greater thereafter. In Table IV, significant errors occur when the core size becomes as small as $r_1 = 0.01$ μm. This is not surprising, as it only means that the core, even though absorbing, is too small to absorb enough radiation to smooth out the oscillations in the internal electric field intensity which are present in the absence of the core. In fact, the electric field intensity at the center, and hence the absorption for such a tiny absorbing inclusion, is a sensitive function of radius a_2 (see refs. 21 and 22).

Table IV. Effect of Core Size (a_1) upon Absorption Cross Section per Unit Volume of the Core (m^2/cm^3) for a Single-Layered Sphere[a]

$a_1(\mu m)$	SL	A	M
2.0	0.6395	0.6447	0.6347
1.0	1.386	1.403	1.399
0.5	3.134	3.169	3.135
0.2	9.935	9.434	9.395
0.1	17.24	18.34	18.35[b]
0.5	26.50	24.45	24.39[b]
0.01	27.01	21.56	22.50[b]

[a] $m_1 = 2.0 - i0.66$, $m_2 = 1.33$, $a_2 = 5$ μm. SL, A, and M refer to the results from the boundary value solution, the approximation method [Eq. (6)], and the Monte Carlo procedure ($N_0 = 1{,}000{,}000$), respectively.

[b] Because the absorption cross sections are very small for such low values of the radius a_1, N_0 was increased to 10,000,000.

6. MONTE CARLO SIMULATION OF SCATTERING BY A DIELECTRIC SPHERE WITH AN INCLUSION AT THE CENTER

Figure 8 traces rays through a single-layered sphere. The outer sphere, of radius a_2, is assumed to be nonabsorbing, while the inner sphere, of radius a_1, may be absorbing. In order to apply the Monte Carlo procedure based on the results of the preceding section, we adopt the following picture. (i) Only those refracted rays which come within the radial distance a_1' interact with the core, where

$$\pi(a_1')^2 = \sigma_{\text{ext}}' \tag{7}$$

and δ_{ext}' is the extinction cross section for the core calculated as if it were embedded in an infinite medium of refractive index m_2. A relative refractive index m_1/m_2 and a wavelength λ_0/m_2, where λ_0 is the wavelength in the outer medium (vacuum), are used in the boundary value theory calculations. The interaction distance a_1' corresponds to impact parameter b_1 for the incident ray, given by

$$b_1 = m_2 a_1' \tag{8}$$

(ii) All other rays with impact parameters greater than b_1 are subject only to geometrical optics.

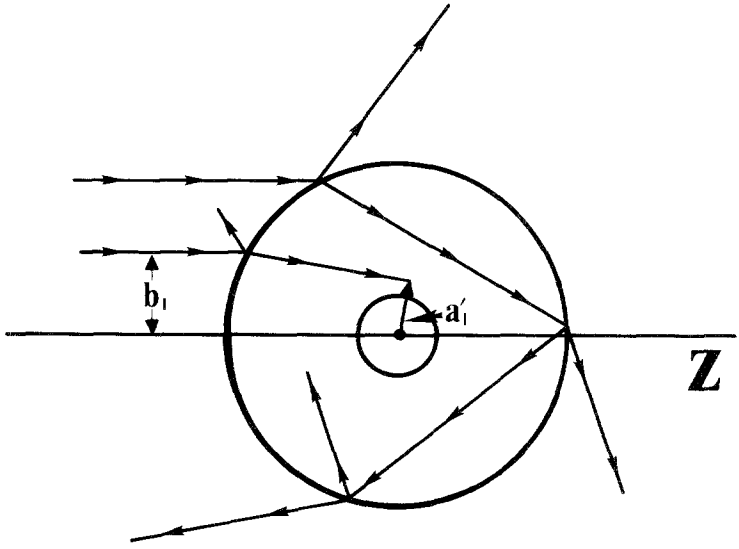

Fig. 8. Ray tracing for scattering by a layered sphere.

The Monte Carlo procedure then consists of the following:

1. The impact parameter of a ray is determined from a random number as discussed earlier ($b_1 = \xi^{1/2} a_2$, $0 < \xi < 1$).

2. This ray is reflected or refracted according to the following rule: (a) $0 < \xi < r^2$, ray is reflected; (b) $r^2 < \xi < 1$, ray is refracted. ξ is a new random number. r is the Fresnel coefficient for the assumed polarization.

3. If (a) is true, the process is terminated, information is stored, and a new ray is generated in step 1.

4. If (b) occurs, two subcases arise: (i) $b < b_1$, (ii) $b > b_1$.

Case (i): The refracted ray interacts with the core. The probability of its being absorbed by the core is given by

$$p_{\text{abs}} = \sigma'_{\text{abs}} / \sigma'_{\text{ext}} \tag{9}$$

where prime, as before, refers to the calculation of quantities for the core within an infinite medium of refractive index m_2. A random number is selected and two subcases again arise: (α) $0 < \xi < p_{\text{abs}}$, ray is absorbed; (β) $p_{\text{abs}} < \xi < 1$, ray is scattered.

Case (α): If this case occurs, information is stored, and the path of a new ray is generated in step 1.

Case (β): If this case occurs, the direction of scattering is determined by numerically solving

$$(\xi)(\sigma'_{\text{sca}}) = \int_0^{\theta} \frac{d\sigma'_{\text{sca}}}{d\theta} \, d\theta \tag{10}$$

θ is measured with respect to the z axis. The scattered ray will strike the surface of the outer sphere normally. This ray may be considered refracted out, or, depending upon the accuracy desired, the above game of chance may be pursued further. The results in Tables III and IV consider the ray refracted out after being scattered by the core, which accounts for the somewhat lower values obtained by the Monte Carlo procedure in comparison with the approximation method, Eq. (6).

The angular scattering efficiency for a layered sphere obtained by the boundary value solution is compared with the Monte Carlo procedure in Fig. 9. These results were obtained by averaging over polarizations 1 and 2.

Once again the lack of structure in the Monte Carlo results is due to failure to include phase and can be rectified were that desired. However, there is general agreement between the two results, including the rainbows near 140° and 130° due to the $p = 2$ and $p = 3$ rays. Accordingly, we are encouraged that this Monte Carlo algorithm provides an accurate representation of the scattering and absorption of light by inhomogeneous particles. It appears feasible to extend the algorithm to less symmetrical

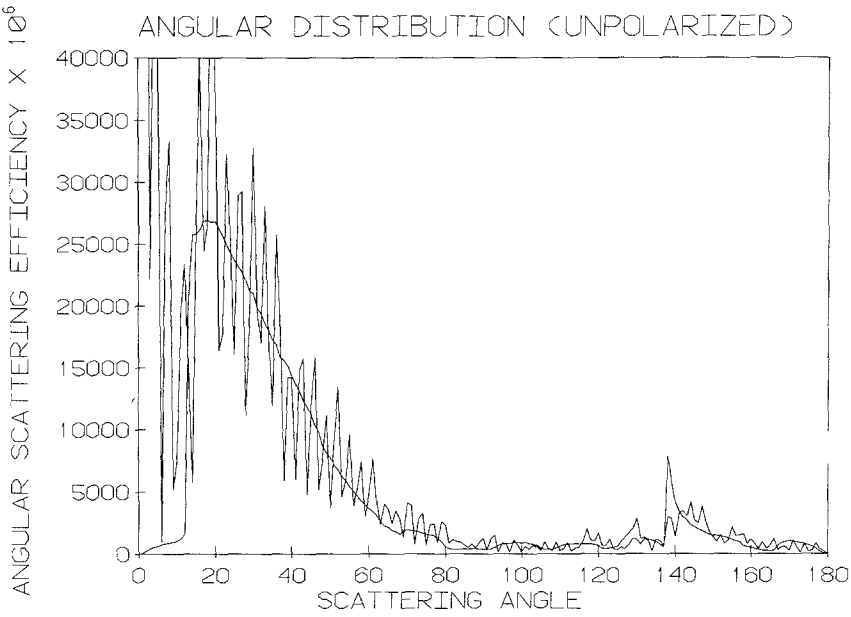

Fig. 9. Comparison of Monte Carlo simulation of scattering with the boundary value solution for a layered sphere, $m_1 = 2.0 - i0.66$, $m_2 = 1.33$, $r_1 = 1$ μm, $r_2 = 5$ μm, $\lambda_0 = 1.33$.

structures for which boundary value solutions cannot be obtained or can be obtained only with difficulty.

Yet, from the practical point of view of performing particle diagnostics, these Monte Carlo results obviously are not promising. There are only small differences upon inserting the core (Fig. 9) into the homogeneous particle (Fig. 6). In one sense this is not surprising, since the 1-μm core represents less than 1 % of the volume. Yet it illustrates the difficulty of utilizing plane wave illumination (zero resolution) to investigate internal structure. For example, there is some enhancement by the core of the intensity of the scattering in the region around 75°. But this averages about 20 %, an effect hardly useful for experimental diagnostics. Uncertainty in particle size or shape would have a greater effect.

However, as will be apparent in the next section, slit-scan illumination may provide the desired resolution for discrimination between homogeneous and heterogeneous particles as well as among various heterogeneous particles.

7. SLIT-SCAN RESULTS

The only modification necessary to convert the algorithm for plane wave illumination used in the previous section to slit-scan illumination is to reject all impinging rays not falling within the beam depicted in Fig. 3. A scattering diagram is then obtained for various positions of the slit from grazing position as it enters the particle to a similar position upon exit.

Figure 10 represents the power received at the detector in the yz plane when the central ray received by the detector is 73° for a 5-μm homogeneous particle. For slit-scan detection, the geometry of the detector plays a significant role. In this case, the detector subtends a solid angle of 5×10^{-3} steradians. The abscissa in Fig. 10 represents the location of the center of the beam relative to the particle center. The enhanced scattering as the beam sweeps across the particle surface is due first to the $p = 0$ rays (see Fig. 5), which reflect off the outer surface, and then to the $p = 1$ rays, which undergo one internal reflection. The asymmetry, as well as the reduced intensity when the beam is entirely within the particle, arises from the detector geometry and varies with the location of the detector. In this case once the beam is entirely within the particle, none of the radiation is intercepted by the detector. This slit-scan contour clearly depicts the particle diameter. If two detectors were placed symmetrically around the z axis in the yz plane and averaged, the slit-scan contour would be symmetrical

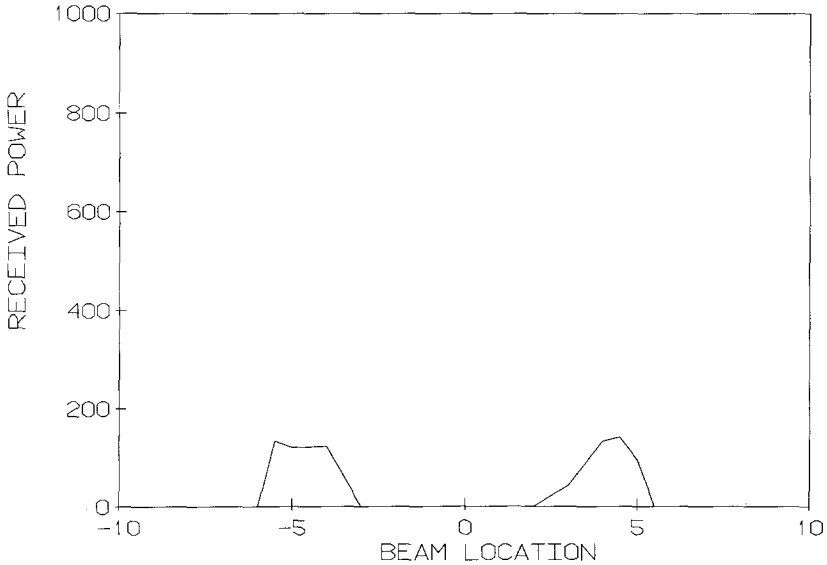

Fig. 10. Slit-scan contour in the yz plane at $\theta = 73°$ for a homogeneous sphere, $r = 5$ μm, $m = 1.33$, $h = 2$ μm.

and the spacing between the two peaks would provide a precise measure of the particle diameter.

The efficacy of the slit-scan technique in displaying the core is illustrated in Fig. 11. The core and host particle radii are $a_1 = 1\ \mu m$, $a_2 = 5\ \mu m$; $m_1 = 2.0 - i0.001$, $m_2 = 1.33$. The wavelength is $0.5\ \mu m$, the height of the slit $h = 2\ \mu m$.

The burst of scattered radiation as the core traverses the beam is dramatic. Because of the discrete spacing in this calculation of the beam positions, the onset of this burst cannot be precisely localized. It appears to occur when the center of the beam is about 2.5–3.0 μm from the edge. With an extinction cross section of $\sigma_{ext} = 2.6$ and a beam height $h = 2\ \mu m$ this would be predicted to occur at 2.8 μm from the center. It should be noted that interaction with the core occurs at a distance a_1' (Fig. 8) determined by the extinction cross section rather than at a_1, the geometrical cross section. Since the excess a_1' over a_1 is mainly in the diffracted radiation, the effect may be quite small in the lateral scattering direction. This aspect requires further study.

8. CONCLUSION

The scattering and absorption by a layered particle consisting of an absorbing sphere at the center of a larger dielectric host has been treated

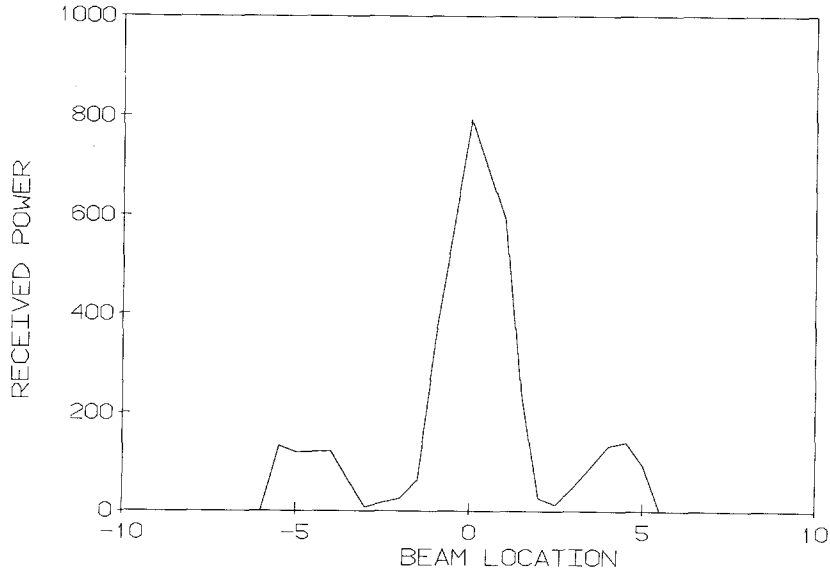

Fig. 11. Slit-scan contour in the yz plane at $\theta = 73°$ for a layered sphere, $a_1 = 1\ \mu m$, $a_2 = 5\ \mu m$, $m_1 = 2.0 - i0.66$, $m_2 = 1.33$, $h = 2\ \mu m$.

by a Monte Carlo technique for which interaction with the host is treated by geometrical optics while interaction with the core is treated by the full boundary value solution. The algorithm which includes both the geometrical optics and the Monte Carlo approximations has been tested by comparison with the scattering and absorption obtained by the boundary value theory for both a homogeneous and a layered sphere.

The procedure is readily adapted to slit-scan illumination and for this technique the effect of the core on the scattering signals is dramatically enhanced.

In future work the algorithm will be extended to include one or more inclusions located off-center, with a view to illustrating effects that might be encountered in experimental studies with biological and meteorological systems.

ACKNOWLEDGMENTS

This work has been supported by ARO grant DAAG29-85-K-0102 and NIH grant RO1CA45246-01. One of the authors (M.K.) acknowledges with appreciation that Prof. Leon L. Wheeless first brought the problem of slit-scan illumination to his attention.

REFERENCES

1. J. W. Strutt, *Scientific Papers* (Cambridge University Press, Cambridge, 1899–1920) [Reprinted, Dover, New York, 1964].
2. M. Kerker, *Selected Papers on Light Scattering* (SPIE, Bellingham, Washington, 1988).
3. M. Bartholdi, G. C. Salzman, R. D. Hiebert, and M. Kerker, *Appl. Opt.* **19**:1573 (1980).
4. P. J. Wyatt, K. L. Schehrer, S. D. Phillips, C. Jackson, Y.-J. Change, R. G. Parker, D. T. Phillips, and J. R. Bottinger, *Appl. Opt.* **27**:217 (1988).
5. J. A. Steinkamp, *Rev. Sci. Instrum.* **55**:1375 (1984).
6. M. R. Melamed, P. F. Mullaney, and M. R. Mendelsohn, eds., *Flow Cytometry and Sorting* (Wiley, New York, 1979).
7. A. L. Aden and M. Kerker, *J. Appl. Phys.* **22**:1242 (1951).
8. P. J. Wyatt, *Appl. Opt.* **7**:1879 (1968).
9. A. Brunsting and P. F. Mullaney, *Appl. Opt.* **11**:675 (1972).
10. R. W. Fenn and H. Oser, *Appl. Opt.* **4**:1504 (1965).
11. R. Bhandari and P. Chylek, *J. Opt. Soc. Am.* **A1**:1236 (1984).
12. M. Sitarski, *Langmuir* **3**:85 (1987).
13. M. Kerker, D. D. Cooke, H. Chew, and M. Kerker, *J. Opt. Soc. Am.* **68**:592 (1978).
14. D. S. Saxon, *Phys. Rev.* **100**:1771 (1955).
15. P. Chylek, V. Ramaswamy, and R. J. Chang, *J. Atmos. Phys.* **41**:3076 (1984).
16. C. F. Bohren, *J. Atmos. Phys.* **43**:468 (1986).
17. L. L. Wheeless and S. F. Patten, *Acta Cytol.* **17**:333 (1973).

18. L. L. Wheeless, T. K. Berkan, S. F. Patten, J. E. Reeder, R. D. Robinson, M. M. Eldidi, W. C. Hulburt, and I. N. Frank, *Cytometry* **7**:212 (1986).
19. H. C. van de Hulst, *Light Scattering by Small Particles* (Wiley, New York, 1957), Chapter 12.
20. M. Kerker, *The Scattering of Light and Other Electromagnetic Radiation* (Academic Press, New York, 1969).
21. R. Bhandari, *J. Opt. Soc. Am.* **3**:319 (1986).
22. R. Bhandari, *Appl. Opt.* **25**:3331 (1986).